Contribution of Thermal Neutrons to Soft Error Rate

Cécile Weulersse, Sabrine Houssany, Nicolas Guibbaud, Jaime Segura-Ruiz, Jérôme Beaucour, Florent Miller and Maria-Magdalena Mazurek

***Abstract*— Boron-10 is part of the fabrication process for a high number of memory and logic devices below 65 nm and the reaction of low-energy cosmic neutrons with high concentrations of B10 in the device contributes to the soft error rate. Based on experiments at ILL facility, the thermal neutron contribution of 3 devices (one SRAM, one FPGA and one microprocessor) is investigated for both ground level and aircraft environments. We conclude that the thermal neutron induced SEUs could have a similar contribution to soft error rate than the high-energy part in atmospheric applications.**

***Index Terms*—Single Event Effect, Soft Error, Thermal neutrons.**

I. Introduction

THERMAL neutrons are high energetic neutrons which have lost kinetic energy, by environmental material scattering, down to an average energy of 25 meV in equilibrium with room temperature. Thermal neutrons interact with the device only through exothermic or exo-energetic reactions. Only a few isotopes show cross sections with thermal neutrons high enough to significantly impact soft error rates (SER). One such isotope is the Boron-10 (B10), with a natural abundance of about 20% and a thermal neutron capture cross section that is orders of magnitude higher than that of most other isotopes present in semiconductor materials (cross sectional area is 3838 barns) and the particularity that B10 nucleus breaks apart [1]. The fission byproducts (including an alpha particle and a lithium-7 nucleus with range in silicon of ~5 µm and ~3µm respectively) may change the logic state of a cell, phenomenon known as a Single Event Upset (SEU).

During the late 1990s, thermal neutrons were a serious source of soft errors in SRAMs and DRAMs fabricated with Borophosphosilicate glass (BPSG) used as dielectric, leading to an increase of the SER by up to x8 [2-7]. More recently, IC manufacturers totally removed BPSG and therefore the SER due to thermal neutrons decreased.

However, B10 remains present at silicon level through p-type dopant source/drain implantation. A wide disparity (a variation of up to x400) is observed in the thermal neutron SEU response of the devices that eliminate BPSG layer [7].

Above all, some SRAM memories in technologies below 90 nm that do not contain BPSG exhibit a relatively high sensitivity to thermal neutrons, mostly correlated to a high concentration of B10 in tungsten plug layer due to novel backend interconnect process options [8-10]. For instance, significant amounts of B10 originate from B_2H_6 or BCl_3 etcher gas for metal process [11-14]. Sensitivity is specific to particular fabs, not to a whole process size [8,11].

The lesson learnt from this discovery is that all new process flow should be inspected to ensure that high levels of B10 do not contaminate chip layers [1]. As a consequence, thermal neutron SEU mitigation techniques were implemented for some 20 nm FPGAs through process modification and were able to reduce the CRAM SEU cross section by ~ 80X [15].

Few papers relate thermal neutron characterization on FinFET devices and scaling effect [16-19]. Both Flip-Flop and SRAM thermal neutron SER decrease as technology scales. Thermal neutron contributions compared to neutrons SER were reported to be the same order of magnitude among founders, from 10 to 20% contributions at sea level for FinFET devices, except for some Flip-Flop designs for which thermal neutrons contribution exceed 30% [19].

Power MOSFETs and IGBTs also experienced burnout events in the thermal neutron environment, most likely caused by boron dopant used in the p-body region [20-21].

At present, the large majority of recent devices which have been reported to be tested towards thermal neutrons were SRAM components, except for logic flip-flop test chips in [13,19] and FPGAs in [15]. In this study, we present data on a SRAM memory, a FPGA and a microprocessor. After discussing the thermal neutron flux and fraction in atmospheric environments, we detail the thermal neutron test performed on the 3 devices. Then, we examine the thermal neutrons induced SEU rate compared to the SEU threat from the high-energy neutrons.

II. Natural Environments

A. At ground level

The thermal neutron flux scales with geomagnetic latitude/longitude and with altitude in a manner similar to the flux of incident energetic cosmic rays. But while the shape of the neutron flux above a few MeV is nearly constant, the shape in the epithermal region, and especially in the thermal energy band, depends on the local environment and building materials, because neutrons up to 1 MeV come partly from scatter in surrounding materials.

Manuscript received April 24, 2017; revised September 29, 2017.

C. Weulersse is with Airbus Group Innovations, 31025 Toulouse, France (e-mail: cecile.weulersse@airbus.com).

S. Houssany and N. Guibbaud were with Airbus Group Innovations, 92150 Suresnes, France, now are with Airbus Defence and Space, 78996 Elancourt, France.

J. Segura and J. Beaucour are with Institut Laue-Langevin/IRT Nanoelec, 38042 Grenoble, France.

F. Miller was with Airbus Group Innovations, 92150 Suresnes, France, now is with Nuclétudes, 91978 Les Ulis, France.

M.-M. Mazurek is with Airbus Operations SAS, 31060 Toulouse, France.

Several ground-based measurements managed to characterize the thermal neutron part of the cosmic rays at numerous locations, outdoor and inside buildings, over and under water, in all weather conditions, over the solar year and as a function of seasonal oscillations [22-26]. During intense rainstorms, the thermalized neutron flux doubles [23]. A thick layer of snow provokes a sharp decrease in the thermal fluence rate [26]. According to the measurements performed by Dirk *et al* in Annapolis, US [22], the unattenuated ambient terrestrial thermal flux ranges from 3.9 to 9.9 n/cm^2/h at sea level.

In JEDEC JESD89A [27], the reference value for the thermal energies (<0.4 eV) flux at New York City (sea level) outdoors for a mean solar activity is 6.5 n/cm^2/h. This value is the average of the two sets of measurements described in [23-24] after scaling to the reference conditions. This flux is relatively important compared to the neutron flux above 10 MeV (13 n/cm^2/h). This leads to a ratio of 0.5 between the thermal neutron flux and the high-energy neutron flux.

Indoors, the shielding materials reduce both thermal and high-energy neutron fluxes. The thermal flux is more quickly attenuated by building materials than in the higher energy part. The exception is that a small amount of material increases the thermal flux by moderating faster neutrons present in the environment [22].

For medical applications, the thermal neutron environment near high-energy cancer radiotherapy may be 4×10^7 higher compared to natural environment [28].

B. Aircraft environments

Commercial aircrafts operate at altitudes of 40,000 feet, where the flux density is approximately 300 times greater than at sea level. In comparison to seal level, the thermal neutron flux in the atmosphere is relatively low due to absorption by atmospheric molecular nitrogen and may be a factor of 0.15 to 0. 25 times the high-energy neutron flux [29-31].

The high-energy neutron flux within an aircraft is essentially the same as the flux in the atmosphere outside the aircraft structure. This is not true for the thermal energies. The presence of hydrogenous materials (fuel, baggage, passengers, etc.) that thermalize higher energy neutrons entering from the atmosphere produces more thermal neutrons within the airplane than that are present outside. It appears that the thermal neutron flux inside an airliner may be 1 to 2 times the high energy (> 10 MeV) neutron flux [30, 32]. However, materials contained within an airliner are non-uniformly distributed, and the thermal neutron environments within a large airliner are thus difficult to predict. Moreover, measurements performed inside airliners have been rare concerning low-energy neutrons and the thermal neutron environment is not well defined [30].

Based on the most applicable set of in-flight measurements, for civil aircraft, the international standard IEC proposes a value of 0.5 for the ratio of the thermal to high-energy neutron flux, though a lack of confidence remains around this figure [30]. Moreover, according to the one detailed calculation that has been carried out for a crudely modelled 747 [32], it has been shown that at several locations within an aeroplane, the thermal fraction increases by more than a factor of 10, leading to a ratio of 1.75 between thermal and high-energy neutrons [29]. Consequently, IEC proposes to use an average between the values of 0.5 and 1.75, which is considered as 1.1, for the value of ratio [29-30]. As stated in the conclusion of the simulation study of [32], it is also possible that there are some locations within an airliner where this ratio can be as large as 2 or higher.

III. RADIATION TESTING

We conducted thermal neutron experiments at the Platform for Advanced Characterisation (PAC-G) facility hosted by the Institut Laue-Langevin (ILL) on 3 chips from different nodes to highlight the phenomenon of thermal neutron susceptibility on advanced process technologies.

A. Thermal neutron facility

The tests were carried out using the PAC-G instrument D50 (see Figure 1) at the ILL site in Grenoble (France) [33]. The ILL is the world leading neutron facility operating a very high flux 60 MW nuclear reactor. D50 is a multi-technique instrument fully dedicated to industrial activity. It offers three neutron techniques among those mainly demanded by the industry: neutron reflectivity, neutron irradiation, and neutron tomography, with resolution in the range of a few microns. The neutrons available on D50 are produced by the ILL horizontal cold source (thermal neutrons moderated by liquid deuterium at 20°K) and transmitted along a 100 m long n-guide. The captured flux (i.e. equivalent flux of 25 meV neutrons) delivered on D50 is adjustable from 0 to 10^{10} n/cm^2/s, with an automatized adjustment for a flux range from 10^6 n/cm^2/s to 10^8 n/cm^2/s. A 5 mm thick graphite block is placed in the beam path in order to improve the beam-profile homogeneity (shown in Figure 1). The neutron spectrum, also shown in Figure 1, shows an energy range from few meV to around 100 meV, with a maximum flux around 13 meV. The neutron spot size may be easily adapted from local irradiation (0.2x0.2 mm^2) to global irradiation (about 160x160 mm^2) by means of motorized borated carbon (B4C) slits. The neutron beam homogeneity can be measured in real time with dedicated LiF/ZnS scintillator-based detector, and/or periodical gold foil measurements to achieve absolute flux data.

B. DUTs

Three packaged devices were irradiated under thermal neutron beam with a spot size of 100 mm^2. For all of the tested devices, a checkerboard pattern was used and a total fluence of $5\text{x}10^{10}$ to $1\text{x}10^{11}$ neutrons/cm^2 was achieved. All devices were tested under nominal temperature and voltages.

The first one is a 4 Mbit SRAM (CY7C1049DV33) from Cypress laid out on a CMOS bulk 90 nm technology. This device has already been irradiated using high-energy protons at UCL (Belgium) and 14 MeV neutrons at the SODERN facility (France). More than 150 SEUs on 2 samples were collected.

The second one is a SRAM-based FPGA previously tested towards high-energy protons, atmospheric neutrons and 14 MeV neutrons at GENEPI2 facility (Grenoble). The radiation behavior of the CLB (Configurable Logic Block) and block RAM (BRAM) cells built in a 45 nm bulk process were

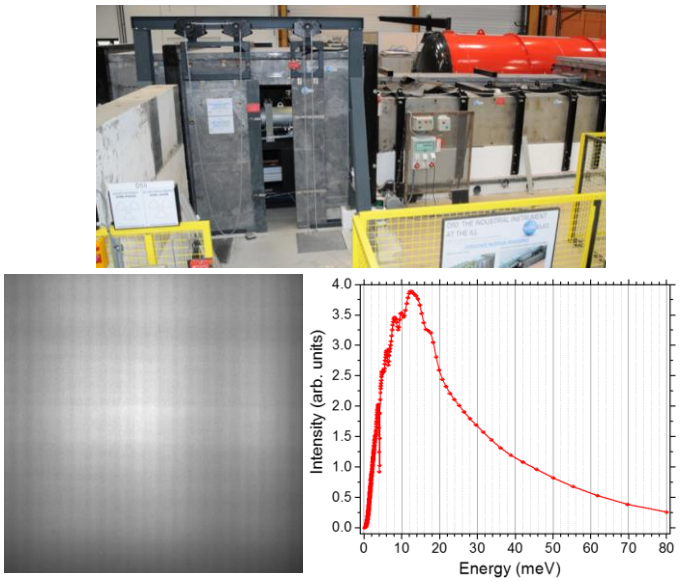

Fig. 1. Picture of the D50 facility (top), 80x80 mm2 beam-profile image (left) and real time energy spectrum of the neutron beam (right).

analyzed. The duration of the FPGA READBACK is around 110 ms. About 600 SEUs were triggered.

Finally, a 28 nm bulk CMOS microprocessor, formerly investigated towards protons, was also irradiated to thermal neutrons in a stand-by configuration, in order to evaluate the L1 data cache (32 kB), L1 instruction cache (32 kB) and L2 cache (256 kB) static cross sections. During the irradiations, all the protection mechanisms were deactivated and the different elements of the cache were monitored: the tag array, the data array and the status bits.

Testing was performed using a development board controlled through a JTAG probe. The content of all cells was continuously read during the irradiations. A total of 2200 upsets were recorded over the duration of the experiments.

IV. Analysis

The FIT calculation is based on the methodology proposed by Zhang *et al.*, which pointed out the importance of calculation of effective flux and shielding effects of package materials [9]. For energies below 100 keV, the B10 neutron capture cross-section increases with decreasing energy, varying as $E^{-1/2}$. The two ions emitted during the reactions have energies which are quasi-independent of the neutron energy from 1 meV to 1 keV. The changes in the neutron spectra after crossing the packaging-material were evaluated thanks to Geant4 based simulations. We thus express the flux of the spectrum that each device receives during irradiations in terms of equivalence to a mono-energetic neutron at 25.8 meV.

Table 1 provides the experimental cross sections obtained at ILL under thermal neutrons as well as radiation data gathered at UCL (Belgium) using high-energy protons and at TSL (Sweden) with atmospheric-like neutrons. For thermal neutron cross sections, the experimental values were corrected, taking into account the efficiency of ^{10}B capture cross-section and the package effect. For high-energy neutrons, the values of the both cross sections were calculated by considering the TSL

TABLE I
Experimental Cross Sections

SEU cross section (cm^2/bit)	Thermal neutrons 25.8 meV (ILL-D50)	60 MeV protons (UCL)	Atmospheric neutrons (TSL)
90 nm SRAM	$3.9x10^{-16}$	$1.5\ x10^{-14}$	/
45 nm CLB	$2.7\ x10^{-15}$	$9.6\ x10^{-15}$	$9.8\ x10^{-15}$
45 nm BRAM	$1.2\ x10^{-14}$	$2.2\ x10^{-14}$	$2.4\ x10^{-14}$
28nm µprocessor	$9.4\ x10^{-15}$	$6.8\ x10^{-15}$	/

TABLE II
Estimation of Soft Error Rate

	SER (FIT/Mbit)		Thermal neutron contribution to neutron SER	
	Thermal neutrons at sea level	High-energy neutrons at sea level	At sea level	At 40,000 feet (12 km) inside aircraft
90 nm SRAM	3	195	1%	3%
45 nm CLB	17	125	12%	24%
45 nm BRAM	75	290	21%	37%
28nm µprocessor	61	88* 136**	41%* 31%**	60%* 50%**

Based on high-energy neutron flux >10 MeV for * and >1 MeV for **

neutron part above 10 MeV. The ANITA beam at TSL is specified to be a low thermal neutron flux (<1% of the integrated flux). In FPGAs, the BRAM cells are often built in a more aggressive technology than most of the CLB cells. This can explain the highest sensitivity of BRAM cells to thermal neutrons obtained during our experiments. On the 28 nm devices, the data cache L1, the instruction cache L1 and the cache L2 share almost the same data sensitivity, for both thermal and high-energy neutrons. These values represent raw static cross sections and do not take into account the derating factor due to the mitigations or dynamic behavior of the processor. More than 95% of upset are due to data. No MBU were induced. We also observed an event similar to a SEFI in the CPU: the JTAG could not access to the cache memories.

Table 2 gives the estimation of soft error rate at sea level. We use the standardized thermal neutron rate 6.5 n/cm^2/h from the JEDEC standard specification [27]. For the high-energy part, a cumulative flux gives 13 n/cm^2/h for neutrons over 10 MeV and a flux of 20 n/cm^2/h over 1 MeV. For the 90 nm memory, the SEU rate at sea level was assumed to be mostly induced by neutron above 10 MeV. For 45 nm cells, the SER was based on data from a white neutron beam spectrum (TSL). Thus neutron threshold energy has a low effect on estimated SER, if we presume a good fidelity of neutron beam spectra at TSL compared to the reference spectrum at ground level between 1 and 10 MeV. For the 28 nm target, calculations based on both neutron threshold energies (>10 MeV and >1 MeV) are provided.

Table 2 also shows the thermal neutron contribution to neutron soft error at sea level and at aircraft altitudes. For the 28 nm feature size, the thermal neutron contribution at sea level ranges from 31% to 41%, which is higher than the data of ~10% given in [8] for a similar technology. For avionic applications, based on the ratio of 1.1 between thermal and high-energy neutrons inside an aircraft, the SER caused by thermal neutrons is less than 3% of the cosmic-ray high-

energy neutron SER on the 90 nm SRAM device we tested, but reached 37% on the 45 nm BRAM cells and 50 to 60% on the cache cells of the 28 nm µprocessor.

V. Conclusion

In this paper, the increase of the thermal neutron susceptibility between a 90 nm component and a sub-65nm one is confirmed. The contribution of the terrestrial thermal neutrons was found to be non-negligible and should not be ignored. On the 28 nm device, for avionic applications, this contribution is equivalent to the one from the high-energy part.

At the present time, IEC standards recommend to take a margin of 7.6X on the high-energy neutrons SEU rate, for devices with feature sizes above 100 nm which may potentially contain B10 and which have not been tested under thermal neutrons [30]. This value is based on a worst case value of 6 obtained on a 250 µm SRAM which certainly contained B10 in the BPSG. Our results show that the proposal of IEC standards is a very conservative approach, due to two sources of uncertainty. The first uncertainty concerns the thermal sensitivity of advanced integrated circuits because of a lack of data and a large variation between manufacturer and fabs.. Our study emphasizes the need of thermal neutron testing to lower the margin proposed by IEC while still considering the growing B10 concern. The second uncertainty deals with environment. This shows the importance of better estimating the variation of neutron flux inside of aircraft and confirming by measurements the 10X increase. As pointed out in [30], new simulations focusing on locations where the electronics are placed would be needed to calculate the thermal neutron flux accurately.

VI. Acknowledgment

The authors wish to thank Kalvin Buckley of ILL for the great help during the neutron experiments. Part of this study was funded by the DEMETER project (ENIAC/ECSEL JU funding). Part of the beamtime on D50 was allocated by the IRT Nanoelec, supported by the French State in the frame of the program “Investissements d’Avenir”, under the reference ANR-10-AIRT-05.

References

[1] R. C. Baumann, “Landmarks terrestrial Single-Event Effects,” 2013 NSREC Short Course.

[2] T. Oldham, S. Murrill, and C. T. Self, “Single event upset of VLSI Memory Circuits Induced by Thermal Neutrons,” *Radiation Effects, Research and Engineering*, vol. 5, no. 1, p. 6, 1986.

[3] R. C. Baumann, T. Z. Hossain, E. Smith, S. Murata, and H. Kitagawa, “Boron as a primary source of radiation in high density DRAMs,” *Proc. IEEE Symp. VLSI Tech*, Jun. 1995, pp. 81–82.

[4] R. C. Baumann and E. B. Smith, “Neutron-induced ^{10}B fission as a major source of soft errors in high density SRAM’s,” *Microelectronics Reliability*, vol. 41, pp.211-218, 2001.

[5] E. Normand, K. Vranish, A. Sheets, M. Stitt, and R. Kim, “Quantifying the double-sided neutron SEU threat, from low energy (thermal) and high energy (>10MeV) neutrons,” *IEEE Trans. Nucl. Sci.*, vol. 53, no. 6, pp.3587–3595, Dec. 2006.

[6] T. Granlund and N. Olsson, “SEUs induced by thermal to high-energy neutrons in SRAMs,” *IEEE Trans. Nucl. Sci*., vol. 53, no. 6, pp. 3798–3802, Dec. 2006.

[7] M. Olmos, R. Gaillard, A. Van Overberghe, J. Beaucour, S. Wen, and S. Chung, “Investigation of thermal neutron induced soft error rates in commercial SRAMs with 0.35 µm to 90 nm technologies,” *Proc. IEEE Int. Reliab. Phys. Symp.*, 2006, pp. 212–216.

[8] S. Wen, R. Wong, M. Romain, and N. Tam, “Thermal neutron soft error rate for SRAM in the 90-45 nm technology range,” *Proc. IEEE Int. Reliab. Phys. Symp.*, 2010, pp. 1036–1039.

[9] M. Zhang, J. Park, G. Kim, K. S. Kim, R. Gaillard, E. Schaefer, and O. Lauzeral, “Thermal neutron SER testing and analysis: findings from a 32nm HKMG SRAM case study,” *Proc. SELSE Worskhop*, Mar. 2011, pp. 1–8.

[10] J. L. Autran, S. Serre, S. Semikh, D. Munteanu, G. Gasiot, and P. Roche, “Soft error rate induced by thermal and low energy neutrons in 40 nm SRAMs,” *IEEE Trans. Nucl. Sci.*, vol. 59, no. 6, pp. 2658–2665, Dec. 2012.

[11] S. J. Wen, S. Y. Pai, R. Wong, M. Romain, and N. Tam, “B10 findings and correlation to thermal neutron soft error rate sensitivity for SRAMs in the sub-micron technology,” *Proc. IEEE Int. Integrated Reliab. Workshop*, 2010, pp. 31–33.

[12] http://www.ineer.org/Events/ICEEiCEER2009/full_papers/full_paper_189.pdf

[13] Y.-P. Fang and A. S. Oates, “Thermal neutron-induced soft errors in advanced memory and logic devices,” *IEEE Trans. Device Mater. Rel.*, vol. 14, no. 1, pp. 583–586, 2014.

[14] J. Park *et al*, “Development of thermal neutron SER-resilient high-K/metal gate technology,” *Proc. IEEE Int. Reliability Phys. Symp.*, 2014.

[15] P. Maillard, M. Hart; J. Barton, P. Jain, and J. Karp, “Neutron, 64 MeV proton, thermal neutron and alpha single-event upset characterization of Xilinx 20nm Ultrascale Kintex FPGA,” *Proc. IEEE Radiation Effects Data Workshop*, Jul. 2015, pp. 228–232.

[16] N. Seifert, S. Jahinuzzaman, J. Velamama, R. Ascazubi, N. Patel, B. Gill, J. Basile, and J. Hicks, “Soft error rate improvements in 14-nm technology featuring second generation 3D tri-gate transistors,” *IEEE Trans. Nucl. Sci*., vol. 62, no. 6, pp. 2570–2577, Dec. 2015.

[17] S. Lee, I. Kim, S. Ha, C-S. Yu, J. Noh, S. Pae, and J. Park, “Radiation-induced soft error rate analyses for 14 nm FinFET SRAM devices,” *Proc. IEEE Int. Reliab. Phys. Symp*., 2015.

[18] Y.-P. Fang and A. S. Oates, “Characterization of Single Bit and Multiple Cell Soft Error Events in Planar and FinFET SRAMs,” *IEEE Trans. Device Mater. Rel.*, vol. 16, no. 2, pp. 132–137, Jun. 2016.

[19] H. Zhang, H. Jiang, J. D. Brockman, T. R. Assis, X. Fan, B. L. Bhuva, B. Narasimhan, S.-J. Wen and R. Wong, “Thermal neutron-induced soft-error rates for flip-flop designs in 16-nm bulk FinFET technology,” *Proc. IEEE Int. Reliab. Phys. Symp.*, 2017.

[20] A. Hands, P. Morris, K. Ryden, C. Dyer, P. Truscott, A. Chugg, and S. Parker, “Single event effects in power MOSFETs due to atmospheric and thermal neutrons,” *IEEE Trans. Nucl. Sci*., vol. 58, no. 6, pp. 2687–2694, Dec. 2011.

[21] D. Lambert, F. Desnoyers, D. Thouvenot, and B. Azaïs, “Single event effects in power MOSFETs and IGBTs due to 14 MeV and 25 meV neutrons,” *Proc. IEEE Radiation Effects Data Workshop*, Jul. 2014, pp. 77–84.

[22] J. D. Dirk, “Electronic reliability and the environmental thermal neutron flux,” U.S.N.A. Trident Scholar project report no. 291, May 2002.

[23] J. D. Dirk, M. E. Nelson, J. F. Ziegler, A. Thompson, and T. H. Zabel, “Terrestrial thermal neutrons,” *IEEE Trans. Nucl. Sci*., vol. 50, no. 6, pp. 2060–2064, Dec. 2003.

[24] M. S. Gordon, P. Goldhagen, K. P. Rodbell, T. H. Zabel, H. H. K. Tang, J. M. Clem, and P. Bailey, "Measurement of the flux and energy spectrum of cosmic-ray induced neutrons on the ground," *IEEE Trans. Nucl. Sci*., vol. 51, no. 6, pp. 3427–3434, Dec. 2004.

[25] K. Naher, N. Ikeda, H. Fukuda, H. Iwamoto,Y. Fukui, Y. Koba, M. Imamura, and Y. Uozumi, “Terrestrial neutrons in West zone II building on Ito campus,” Memoirs of the Faculty of Engineering, Kyushu University, vol.69, no.1, Mar. 2009.

[26] G. Hubert, C. A. Federico, M. T. Pazianotto, and O. L. Gonzales, " Long and short-term atmospheric radiation analyses based on coupled measurements at high altitude remote stations and extensive air shower modeling," *Astroparticle Physics*, vol. 74, pp. 27–36, Sept. 2015.

[27] *Measurement and Reporting of Alpha Particle and Terrestrial Cosmic Ray-Induced Soft Errors in Semiconductor Devices*, JEDEC Standard no. 89A (JESD89A), Oct. 2006.

[28] http://ewh.ieee.org/soc/cpmt/presentations/cpmt0910f.pdf

[29] *Process management for avionics – Atmospheric Radiation Effects – Part 1: Accommodation of atmospheric radiation effects via single event*

effects within avionics electronic equipment, Equipment, IEC Tech. Std. 62396-1, Jan. 2016.

[30] *Process management for avionics – Atmospheric Radiation Effects – Part 5: Assessment of thermal neutron fluxes and single event effects in avionics system*s, Equipment, IEC Tech. Std. 62396-5, Aug. 2014.

[31] E. Normand, K. V. Vranish, A. Sheets, M. Stitt, and R. Kim, "Quantifying the double-sided neutron SEU threat, from low energy (thermal) and high energy (>10 MeV) neutrons," *IEEE Trans. Nucl. Sci*., vol. 53, no. 6, pp. 3587–3595, Dec. 2006.

[32] C. Dyer and F. Lei, "Monte Carlo calculations of the influence on aircraft radiation environments of structures and solar particle events," *IEEE Trans. Nucl. Sci.*, vol. 48, no. 6, pp. 1987–1995, Dec. 2001.

[33] J. Beaucour, J. Segura-Ruiz, B. Giroud, E. Capria, E. Mitchell, C. Curfs, J. C. Royer, M. Baylac, F. Villa, S. Rey, "Grenoble large scale facilities for advanced characterisation of microelectronics devices," 15th European Conference on Radiation and Its Effects on Components and Systems (RADECS), Sept. 2015, pp. 312–315.